Chapter 3

Transient response of collinear Griffith cracks in a functionally graded strip bonded between dissimilar elastic strips under shear impact loading

3.1 Introduction

Due to great strength at high temperatures, strong resilience to wear, corrosion, radiation, etc., and capacity to reduce residual and thermal stresses, a lot of research has been seen in the field of FGMs in recent years. FGMs are utilized as an interlayer between various composite media, which aids in overcoming the drawbacks brought on by the mismatch property of piecewise composite structures. They have also been extensively utilized in engineering as chemical corrosion inhibitor, thermal barrier, etc. For instance, thermal residual stresses in a metal/ceramic composite can be reduced by introducing a FGM layer between the metal and the ceramic. For such FGMs, the composite has flaws including holes, voids, and cracks. It is

uncertain whether these flaws are stable under static-dynamic loads. Generally, dynamic loading makes crack propagation easy due to the transient impact of suddenly applied impact loads. The graded characteristics of FGM have a significant impact on the cracks' dynamic behavior. As a result, it's important to pay attention to the failure mechanism of cracks when subjected to dynamic loading.

Many researchers have looked into the static crack problems in FGMs. To better understand how three collinear Griffith cracks interact with one another in a functionally graded medium under various specific thermal, mechanical, and thermo-mechanical loading scenarios, a study was undertaken in [102]. The problem of an interfacial crack between two elastic half-spaces was investigated in [91] using anti-plane shear loading. The interface crack problem between ceramic and/or FGM coatings and a substrate, under anti-plane shear loading, was researched in [59] for distinct coating models. A new model was proposed in [51] for the approximation study of FGMs with arbitrary variable properties and to address the issue of a crack in a functionally graded coating adhered to a homogeneous substrate under static anti-plane shear loading. A theoretical treatment for two anti-plane collinear cracks that are perpendicular to and on either side of the interface between a functionally graded orthotropic strip and an orthotropic homogeneous substrate was provided in [31]. The series solution method is used in [3, 22] to determine the stress intensity factors for a finite length crack in a non-homogeneous medium by defining a parameter that describes spatial variation in material properties.

Less research has been done on the dynamic behavior of crack problems than on the static ones. In [122], dynamic analysis for a finite-length crack in the FGMs under harmonic stress waves was provided utilizing the Schmidt method. In [66], DSIFs for a FGM crack that was implanted between two elastic layers while being subjected to anti-plane loading were determined. The problem of a subsurface

crack in a non-homogeneous over-coating on the layered half-space subjected to an anti-plane impact load was addressed in [101] under the assumption that the FGM layer was overcoated. A theoretical description of the dynamic behavior of a Griffith crack in functionally graded orthotropic materials under the normal incidence of time-harmonic elastic waves was provided in [71]. For the dynamic analysis of a crack in a FGM between two dissimilar half-planes under anti-plane shear impact stress, theoretical and numerical research is carried out in [4]. For an interfacial crack, the effect of non-homogeneous elastic constants on DSIFs was discussed in [67].

Researchers have recently focused on the dynamic behavior of single fracture problems in non-homogeneous materials, but less research has been done on the corresponding multiple crack problems and their interactions under impact loading applied at the material surface. In [72], the Schmidt technique was used to analyze the dynamic behavior of two collinear cracks in a FGM layer bonded to dissimilar half-planes. A problem involving an anti-plane dynamic fracture with two collinear cracks perpendicular to a weak discontinuous interface point between two elastic materials was taken into consideration in [68]. An orthotropic strip with a functionally graded materials layer that is deteriorated by numerous random cracks under time-harmonic excitation was solved in [76]. With the aid of Volterra type screw dislocation under anti-plane shear impact loading, transient analysis for two different FGM strips with various interface cracks was carried out in [73]. The majority of research was conducted with loads being applied to the cracked surface. The issue of impact loads acting suddenly at the cracked surface is the subject of very few research [66, 67].

In the current work, the effect of anti-plane sudden impact loading on three collinear Griffith cracks in a FGM strip bonded between two equally thicked distinct

elastic strips has been investigated. In terms of the geometry of collinear cracks, one crack is kept at the center and the other two are symmetrically positioned on either side of the central one along the $x-$axis (see Figure 3.1). The composites will presumably have finite thicknesses. An exponential function of thickness is used to express the material properties of FGM. Laplace and Fourier cosine transforms are both employed to solve the mixed initial-boundary value problem. Analytically, those equations can be simplified to a set of integral equations in the Laplace transform domain. DSIFs in the transformed domain are obtained by the numerical solution of this system using the Lobatto-Chebyshev collocation quadrature method. The inverse Laplace transform is used to find the DSIF's expressions in the time domain. The novel aspect of this chapter is that it examines how cracks interact when a sudden impact load is applied to the upper material surface. A graphical comparison of the impact loads operating on the cracked surface and the upper material surface is shown. The graphical depictions of DSMFs to identify the potential for shielding and amplification phenomena as well as the potential for crack arrest resulting from the interaction of collinear fractures are this chapter's standout elements. The transient response of DSMFs aids in the investigation of the places of impact loadings, the axis of the cracks, and the thickness of the strips on the interactions among the collinear cracks that help to protect or damage the composite material.

3.2 Mathematical formulation of the problem

3.2.1 Schematic description

Consider a FGM strip with a thickness of $2h_0$ placed between two distinct elastic strips with thicknesses of h and have a central Griffith crack of length $2a$ and two symmetrically located outer Griffith cracks of the same length $c-b$ along the $x-$axis (see Figure 3.1). The notations (1), (2), and (3) denote the upper elastic, FGM, and lower elastic strips, respectively. The shear moduli and mass densities of strips (1), (2) and (3) are denoted by μ_1, μ_2, μ_3; ρ_1, ρ_2 and ρ_3, respectively and the distance from the middle of the FGM strip is represented by e.

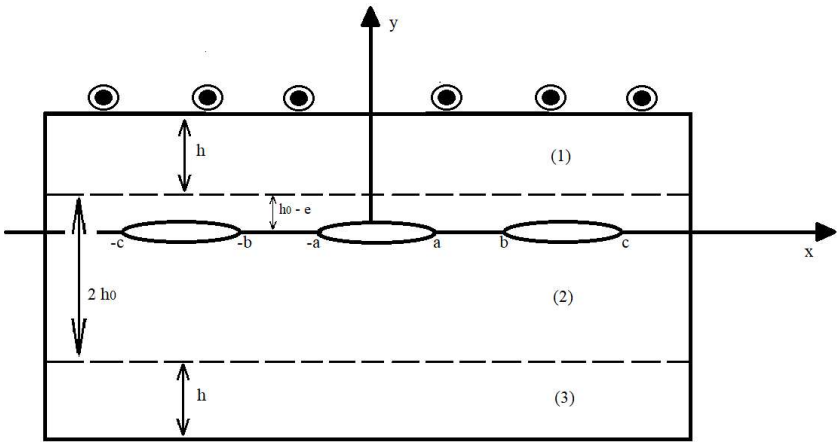

Figure 3.1: Schematic diagram of the problem.

According to Figure 3.1, the upper elastic, the FGM, and the lower elastic strips are located in the regions $\{-\infty < x < \infty,\ (h_0 - e) < y < (h_0 - e + h)\}$, $\{-\infty < x < \infty,\ -(h_0+e) \leq y \leq (h_0-e)\}$ and $\{-\infty < x < \infty,\ -(h_0+e+h) < y < -(h_0+e)\}$, respectively and e lies between $-h_0$ to h_0. It is sufficient to consider the region $\{0 \leq x < \infty,\ -\infty < y < \infty\}$ due to the symmetry of the examined model

about the $y-$axis. The FGM strip's shear modulus is determined by

$$\mu_2 = \mu_3\sqrt{\Gamma^{(e+y+h_0)/h_0}}, \qquad -(h_0+e) \le y \le (h_0-e), \tag{3.1}$$

$$\rho_2 = \rho_3\sqrt{\Gamma^{(e+y+h_0)/h_0}}, \qquad -(h_0+e) \le y \le (h_0-e), \tag{3.2}$$

$$\text{where} \quad \Gamma = \mu_1/\mu_3. \tag{3.3}$$

3.2.2 Governing equations and boundary conditions

Suppose strips (1), (2), and (3) all have the same shear wave velocities, i.e.,

$$C_1 = C_2 = C_3 = c_0(\text{say}), \tag{3.4}$$

$$\text{where} \qquad C_1 = \sqrt{\frac{\mu_1}{\rho_1}}, \qquad C_2 = \sqrt{\frac{\mu_2}{\rho_2}}, \qquad C_3 = \sqrt{\frac{\mu_3}{\rho_3}}. \tag{3.5}$$

$w^{(1)}, w^{(2)}, w^{(3)}$ stand for the displacements and $\sigma^{(1)}, \sigma^{(2)}$, $\sigma^{(3)}$ stand for the dynamic stress fields of strips (1), (2) and (3), respectively. The out-of-plane displacement equations for the upper and lower elastic strips are given by

$$\nabla^2 w^{(i)} - \frac{1}{c_0^2}\frac{\partial^2 w^{(i)}}{\partial t^2} = 0, \qquad i = 1, 3, \tag{3.6}$$

and for the FGM strip, those are given by

$$\nabla^2 w^{(2)} - \frac{1}{c_0^2}\frac{\partial^2 w^{(2)}}{\partial t^2} + \frac{1}{\mu_2}\frac{\partial \mu_2}{\partial y}\frac{\partial w^{(2)}}{\partial y} = 0, \tag{3.7}$$

under the assumptions

$$w^{(i)} = 0, \qquad \frac{\partial w^{(i)}}{\partial t} = 0, \qquad t < 0, \quad i = 1, 2, 3. \tag{3.8}$$

The boundary conditions for sudden impact loads acting at the upper material surface are given by

$$\sigma_{yz}^{(1)}(x,(h_0-e+h),t)=\sigma_0(x)f(t), \qquad 0\le x<\infty,\ t>0, \tag{3.9}$$

$$\sigma_{yz}^{(2p)}(x,0,t)=\sigma_{yz}^{(2n)}(x,0,t)=0, \qquad 0\le x\le a,\ b\le x\le c,\ t>0, \tag{3.10}$$

$$\sigma_{yz}^{(3)}(x,-(h_0+e+h),t)=0, \qquad 0\le x<\infty,\ t>0, \tag{3.11}$$

and for impact loads at cracked surfaces, we have

$$\sigma_{yz}^{(1)}(x,(h_0-e+h),t)=0, \qquad 0\le x<\infty,\ t>0, \tag{3.12}$$

$$\sigma_{yz}^{(2p)}(x,0,t)=\sigma_{yz}^{(2n)}(x,0,t)=\sigma_0(x)f(t), \qquad 0\le x\le a,\ b\le x\le c,\ t>0, \tag{3.13}$$

$$\sigma_{yz}^{(3)}(x,-(h_0+e+h),t)=0, \qquad 0\le x<\infty,\ t>0, \tag{3.14}$$

along with the continuity conditions at the interface for both loading positions given by

$$w^{(1)}(x,(h_0-e),t)=w^{(2p)}(x,(h_0-e),t), \qquad 0\le x<\infty,\ t>0, \tag{3.15}$$

$$w^{(2p)}(x,0,t)=w^{(2n)}(x,0,t), \qquad a<x<b,\ x>c,\ t>0, \tag{3.16}$$

$$w^{(2n)}(x,-(h_0+e),t)=w^{(3)}(x,-(h_0+e),t), \qquad 0\le x<\infty,\ t>0, \tag{3.17}$$

$$\sigma^{(1)}(x,(h_0-e),t)=\sigma^{(2p)}(x,(h_0-e),t), \qquad 0\le x<\infty,\ t>0, \tag{3.18}$$

$$\sigma^{(2p)}(x,0,t)=\sigma^{(2n)}(x,0,t), \qquad a<x<b,\ x>c,\ t>0, \tag{3.19}$$

$$\sigma^{(2n)}(x,-(h_0+e),t)=\sigma^{(3)}(x,-(h_0+e),t), \qquad 0\le x<\infty,\ t>0, \tag{3.20}$$

where in general the dynamic stress field for each strip satisfies

$$\sigma_{yz}=\mu\frac{\partial w}{\partial y}, \tag{3.21}$$

$\sigma_0(x)$ denotes magnitude of impact load, $f(t)$ indicates function of time and the notations (2p) and (2n) indicate the portions of FGM strip $y > 0$ and $y < 0$, respectively. When the impact loads are applied at the upper material surface equations (3.9)-(3.11) indicate that the impact loads are acting only at the boundary of upper elastic strip. Similarly, equations (3.12)-(3.14) indicate that application of impact load at the crack surface only. The continuity among the upper elastic strip, upper portion of the cracked FGM strip, lower portion of the cracked FGM strip, lower elastic strips and outside crack region are given by equations (3.15)-(3.20).

3.3 Solution of the problem

The expressions of out-of-plane displacement in the Laplace transformed domain are found by applying Laplace and Fourier cosine transforms to t and x, respectively on both sides of equations (3.6) and (3.7) and using equation (3.1) as

$$w^{(1)*}(x,y,p) = \int_0^\infty (a_1(\tau,p)\,\exp(-\alpha y) + b_1(\tau,p)\,\exp(\alpha y))\cos(\tau x)d\tau,$$
$$(h_0 - e) \le y \le (h_0 - e + h), \tag{3.22}$$
$$w^{(2p)*}(x,y,p) = \int_0^\infty (a_2(\tau,p)\,\exp[-(\beta+\gamma)y] + b_2(\tau,p)\,\exp[(\beta-\gamma)y])\cos(\tau x)d\tau,$$
$$0 \le y \le (h_0 - e), \tag{3.23}$$
$$w^{(2n)*}(x,y,p) = \int_0^\infty (a_3(\tau,p)\,\exp[-(\beta+\gamma)y] + b_3(\tau,p)\,\exp[(\beta-\gamma)y])\cos(\tau x)d\tau,$$
$$-(h_0 + e) \le y \le 0, \tag{3.24}$$
$$w^{(3)*}(x,y,p) = \int_0^\infty (a_4(\tau,p)\,\exp(-\alpha y) + b_4(\tau,p)\,\exp(\alpha y))\cos(\tau x)d\tau,$$
$$-(h_0 + e + h) \le y \le -(h_0 + e), \tag{3.25}$$
$$\text{where} \quad \gamma = \frac{1}{4h_0}\log\Gamma, \quad \alpha = \sqrt{\tau^2 + \frac{p^2}{c_0^2}}, \quad \beta = \sqrt{\gamma^2 + \tau^2 + \frac{p^2}{c_0^2}}, \tag{3.26}$$

τ and p are the parameters corresponding to Fourier and Laplace transforms, respectively and $a_i(\tau,p)$, $b_i(\tau,p)$, $(i=1,2,3,4)$ are arbitrary unknown functions in τ and p.

Using equations (3.22)-(3.25), the equation (3.21) gives

$$\sigma_{yz}^{(1)*}(x,y,p) = -\mu_1 \int_0^\infty \alpha\left(a_1(\tau,p)\,\exp(-\alpha y) - b_1(\tau,p)\,\exp(\alpha y)\right)\cos(\tau x)d\tau,$$
$$(h_0-e) \le y \le (h_0-e+h), \tag{3.27}$$

$$\sigma_{yz}^{(2p)*}(x,y,p) = -\mu_2 \int_0^\infty ((\beta+\gamma)a_2(\tau,p)\,\exp[-(\beta+\gamma)y] - (\beta-\gamma)b_2(\tau,p)\,\exp[(\beta-\gamma)y])$$
$$\times \cos(\tau x)d\tau, \qquad 0 \le y \le (h_0-e), \tag{3.28}$$

$$\sigma_{yz}^{(2n)*}(x,y,p) = -\mu_2 \int_0^\infty ((\beta+\gamma)a_3(\tau,p)\,\exp[-(\beta+\gamma)y] - (\beta-\gamma)b_3(\tau,p)\,\exp[(\beta-\gamma)y])$$
$$\times \cos(\tau x)d\tau, \qquad -(h_0+e) \le y \le 0, \tag{3.29}$$

$$\sigma_{yz}^{(3)*}(x,y,p) = -\mu_3 \int_0^\infty \alpha\left(a_4(\tau,p)\,\exp(-\alpha y) - b_4(\tau,p)\,\exp(\alpha y)\right)\cos(\tau x)d\tau,$$
$$-(h_0+e+h) \le y \le -(h_0+e). \tag{3.30}$$

Let s define a new unknown function as

$$\phi(x,t) = \frac{1}{2}\left[\frac{\partial\left(w^{(2p)}(x,0,t) - w^{(2n)}(x,0,t)\right)}{\partial x}\right]. \tag{3.31}$$

Utilising equation (3.16) and the application of Laplace transform with respect to t in equation (3.31) takes the following form

$$\phi^*(x,p) = \frac{1}{2}\left[\frac{\partial\left(w^{(2p)*}(x,0,p) - w^{(2n)*}(x,0,p)\right)}{\partial x}\right], \tag{3.32}$$

$$\int_0^a \phi^*(x,p)dx + \int_b^c \phi^*(x,p)dx = 0 \quad \text{and} \quad \phi^*(x,p) = 0,\ a < x < b,\ x > c. \tag{3.33}$$

Equations (3.15), (3.17)-(3.20), (3.22)-(3.25), (3.27)-(3.30) and (3.32) give six equations in the Laplace transformed domain as

$$\exp[-\alpha(h_0-e)]a_1(\tau,p)+\ \exp[\alpha(h_0-e)]b_1(\tau,p)$$

$$-\ \exp[-(\beta+\gamma)(h_0-e)]a_2(\tau,p)-\ \exp[(\beta-\gamma)(h_0-e)]b_2(\tau,p)=0, \tag{3.34}$$

$$\alpha\ \exp[-\alpha(h_0-e)]a_1(\tau,p)-\alpha\ \exp[\alpha(h_0-e)]b_1(\tau,p)-(\beta+\gamma)\ \exp[-(\beta+\gamma)(h_0-e)]$$

$$\times\, a_2(\tau,p)+(\beta-\gamma)\ \exp[(\beta-\gamma)(h_0-e)]b_2(\tau,p)=0, \tag{3.35}$$

$$a_2(\tau,p)+b_2(\tau,p)-a_3(\tau,p)-b_3(\tau,p)=-r_1(\tau,p), \tag{3.36}$$

$$(\beta+\gamma)a_2(\tau,p)-(\beta-\gamma)b_2(\tau,p)-(\beta+\gamma)a_3(\tau,p)+(\beta-\gamma)b_3(\tau,p)=0, \tag{3.37}$$

$$-\ \exp[(\beta+\gamma)(h_0+e)]a_3(\tau,p)-\ \exp[-(\beta-\gamma)(h_0+e)]b_3(\tau,p)$$

$$\exp[\alpha(h_0+e)]a_4(\tau,p)+\ \exp[-\alpha(h_0+e)]b_4(\tau,p)=0, \tag{3.38}$$

$$-(\beta+\gamma)\ \exp[(\beta+\gamma)(h_0+e)]a_3(\tau,p)+(\beta-\gamma)\ \exp[-(\beta-\gamma)(h_0+e)]b_3(\tau,p)$$

$$\alpha\ \exp[\alpha(h_0+e)]a_4(\tau,p)-\alpha\ \exp[-\alpha(h_0+e)]b_4(\tau,p)=0, \tag{3.39}$$

$$\text{where}\qquad r_1(\tau,p)=\frac{4}{\pi\tau}\left(\int_0^a\phi^*(s,p)\sin(\tau s)ds+\int_b^c\phi^*(s,p)\sin(\tau s)ds\right). \tag{3.40}$$

Since impact load is applied at two distinct positions, therefore there are the following two possibilities.

Case - I: *When impact load is applied on the upper material surface.*

The application of Laplace transform with respect to t in equations (3.9) and (3.11) give

$$\exp[-\alpha(h_0-e+h)]a_1(\tau,p)-\ \exp[\alpha(h_0-e+h)]b_1(\tau,p)=-r_2, \tag{3.41}$$

$$\exp[\alpha(h_0+e+h)]a_4(\tau,p)-\ \exp[\alpha(h_0+e+h)]b_4(\tau,p)=0, \tag{3.42}$$

$$\text{where}\qquad r_2(\tau,p)=\frac{2}{\pi\alpha\mu_1}f^*(p)\left(\int_0^\infty\sigma_0(s)\cos(\tau s)ds\right). \tag{3.43}$$

Solving equations (3.34)-(3.39), (3.41) and (3.42) the following forms of $a_2(\tau,p)$ and $b_2(\tau,p)$ in terms of $r_1(\tau,p)$ and $r_2(\tau,p)$ are found as

$$a_2(\tau,p) = c_1(\tau,p)r_1(\tau,p) + c_2(\tau,p)r_2(\tau,p), \tag{3.44}$$

$$b_2(\tau,p) = d_1(\tau,p)r_1(\tau,p) + d_2(\tau,p)r_2(\tau,p), \tag{3.45}$$

where $c_i(\tau,p)$, $d_i(\tau,p)$ $(i=1,2)$ are known functions of τ and p [66]. In the Laplace transformed domain, the equation (3.10) reduces to the singular integral equation expressed as

$$\frac{1}{\pi}\int_0^a \left(\frac{1}{s-x}+\frac{1}{s+x}+2R(s,x,p)\right)\phi^*(s,p)ds + \frac{1}{\pi}\int_b^c \left(\frac{1}{s-x}+\frac{1}{s+x}+2R(s,x,p)\right) \times \phi^*(s,p)ds = f^*(p)T_t(x), \qquad 0\le x\le a, \quad b\le x\le c, \tag{3.46}$$

where the expressions of $R(s,x,p)$ and $T_t(x)$ are given in Appendix B. The integration interval in the first term of the left-hand side of equation (3.46) can be extended from $[0,a]$ to $[-a,a]$ using symmetry property which also shows that $\phi^*(x,p)$ is an odd function in x in $[-a,a]$. Thus equation (3.46) takes the form given by

$$\frac{1}{\pi}\int_{-a}^a \left(\frac{1}{s-x}+R(s,x,p)\right)\phi^*(s,p)ds + \frac{1}{\pi}\int_b^c \left(\frac{1}{s-x}+\frac{1}{s+x}+2R(s,x,p)\right) \times \phi^*(s,p)ds = f^*(p)T_t(x), \qquad 0\le x\le a, \quad b\le x\le c. \tag{3.47}$$

Case - II: *When impact load is applied on the cracked surface.*

For this loading position in the Laplace transformed domain, the equations (3.12) and (3.14) give

$$\exp[-\alpha(h_0-e+h)]a_1(\tau,p) - \exp[\alpha(h_0-e+h)]b_1(\tau,p) = 0, \tag{3.48}$$

$$\exp[\alpha(h_0+e+h)]a_4(\tau,p) - \exp[\alpha(h_0+e+h)]b_4(\tau,p) = 0. \tag{3.49}$$

The expressions of $a_2(\tau,p)$ and $b_2(\tau,p)$ in terms of $r_1(\tau,p)$ are obtained by solving equations (3.34)-(3.39), (3.48) and (3.49) as

$$a_2(\tau,p) = c_1(\tau,p)r_1(\tau,p), \tag{3.50}$$

$$b_2(\tau,p) = d_1(\tau,p)r_1(\tau,p), \tag{3.51}$$

where $c_1(\tau,p)$ and $d_1(\tau,p)$ have the analogous form as obtained in Case-I. Using equations (3.50) and (3.51) in equation (3.13) yield a singular integral equation which after using symmetry property gives

$$\frac{1}{\pi}\int_{-a}^{a}\left(\frac{1}{s-x}+R(s,x,p)\right)\phi^*(s,p)ds+\frac{1}{\pi}\int_{b}^{c}\left(\frac{1}{s-x}+\frac{1}{s+x}+2R(s,x,p)\right)$$

$$\times\,\phi^*(s,p)ds = f^*(p)T_c(x), \qquad 0\le x\le a, \quad b\le x\le c, \tag{3.52}$$

where $R(s,x,p)$ has the same form as obtained for Case-I and $T_c(x)$ is given by equation (B.0.4) in Appendix B.

3.3.1 Numerical solution of integral equation

The general form of the singular integral equations (3.47) and (3.52) can be expressed as

$$\frac{1}{\pi}\int_{-a}^{a}\left(\frac{1}{s-x}+R(s,x,p)\right)\phi^*(s,p)ds+\frac{1}{\pi}\int_{b}^{c}\left(\frac{1}{s-x}+\frac{1}{s+x}+2R(s,x,p)\right)\phi^*(s,p)ds$$

$$= f^*(p)T_0(x), \qquad 0\le x\le a, \quad b\le x\le c, \tag{3.53}$$

subjected to the conditions given in equation (3.33), where

$$T_0(x) = \begin{cases} T_t(x), & \text{when impact load is applied at the upper material surface,} \\ T_c(x), & \text{when impact load is applied at the cracked surface.} \end{cases} \tag{3.54}$$

To solve equation (3.53) in the Laplace transformed domain, a numerical approach is considered due to the complex form of the kernel of the considered singular integral equation. For numerical computation let us consider

$$\sigma_0(x) = \sigma_0 H(L - |x|) \quad \text{and} \quad f(x) = H(x), \tag{3.55}$$

where $H(*)$ is the Heaviside unit step function, L is a positive number, and $[-L, L]$ is the region of sudden impacts. Thus equation (3.53) gives

$$\frac{1}{\pi}\int_{-a}^{a}\left(\frac{1}{s-x} + R(s,x,p)\right)\phi^*(s,p)ds + \frac{1}{\pi}\int_{b}^{c}\left(\frac{1}{s-x} + \frac{1}{s+x} + 2R(s,x,p)\right) \times \phi^*(s,p)ds = \frac{T_1(x)}{p}, \qquad 0 \le x \le a, \quad b \le x \le c, \tag{3.56}$$

where $T_1(x)$ is given in equation (B.0.5) of Appendix B. For converting the singular integral equation (3.56) to a system of integral equations let us define

$$\eta_1 = \frac{s}{a}, \quad \xi_1 = \frac{x}{a}, \quad \eta_2 = \frac{2s-(b+c)}{c-b}, \quad \xi_2 = \frac{2x-(b+c)}{c-b}, \tag{3.57}$$

$$\phi^*(s,p) = \begin{cases} \phi_1^*(\eta_1,p), & -1 \le \eta_1 \le 1, \\ \phi_2^*(\eta_2,p), & -1 \le \eta_2 \le 1. \end{cases} \tag{3.58}$$

Thus the equation(3.56) reduces to

$$\frac{1}{\pi}\int_{-1}^{1}\left(\frac{1}{\eta_1-\xi_1} + R_{11}(\eta_1,\xi_1,p)\right)\phi_1^*(\eta_1,p)d\eta_1 + \frac{1}{\pi}\int_{-1}^{1}\left(\frac{1}{\eta_2 - z_{12}(\xi_1)} + \frac{1}{\eta_2 - g_{12}(\xi_1)} + R_{12}(\eta_2,\xi_1,p)\right)\phi_2^*(\eta_2,p)d\eta_2 = \frac{T_{11}(\xi_1)}{p}, \qquad -1 \le \xi_1 \le 1, \tag{3.59}$$

$$\frac{1}{\pi}\int_{-1}^{1}\left(\frac{1}{\eta_1 - z_{21}(\xi_2)} + R_{21}(\eta_1,\xi_2,p)\right)\phi_1^*(\eta_1,p)d\eta_1 + \frac{1}{\pi}\int_{-1}^{1}\left(\frac{1}{\eta_2-\xi_2} + \frac{1}{\eta_2 - g_{22}(\xi_2)} + R_{22}(\eta_2,\xi_2,p)\right)\phi_2^*(\eta_2,p)d\eta_2 = \frac{T_{12}(\xi_2)}{p}, \qquad -1 \le \xi_2 \le 1, \tag{3.60}$$

subjected to

$$\int_{-1}^{1}\phi_1^*(\eta_1,p)d\eta_1 = 0 \quad \text{and} \quad \int_{-1}^{1}\phi_2^*(\eta_2,p)d\eta_2 = 0, \tag{3.61}$$

where $R_{ij}(\eta_j,\xi_i,p)$ $(i,j=1,2)$, $g_{i2}(\xi_i), T_{1i}(\xi_i\ i=1,2)$, $z_{12}(\xi_1)$ and $z_{21}(\xi_2)$ are given in Appendix B. Due to singularity of $\phi_i^*(\eta_i,p)'s$ $(i=1,2)$ at the tips of cracks it is considered that

$$\phi_i^*(\eta_i,p) = \frac{\lambda_0\,\Phi_i(\eta_i,p)}{\sqrt{1-\eta_i^2}}, \qquad i=1,2, \tag{3.62}$$

$$\text{where} \quad \lambda_0 = \begin{cases} \sigma_0/\mu_1, & \text{when impact load acts on upper material surface,} \\ \sigma_0/\mu_2, & \text{when impact load acts on cracked surface.} \end{cases} \tag{3.63}$$

With the aid of the quadrature formula

$$\frac{1}{\pi}\int_{-1}^{1}\frac{1}{\eta_i-\xi_{ij}}\frac{\Phi_i(\eta_i,p)}{\sqrt{1-\eta_i^2}}d\eta_i \simeq \frac{1}{n_i}\sum_{k=0}^{n_i}\frac{\zeta_k\Phi_i(\eta_{ik},p)}{\eta_{ik}-\xi_{ij}}, \qquad i=1,2, \tag{3.64}$$

where $\xi_{ij},\ \eta_{ik},\ \zeta_k$ are given in Appendix B. Approximation of the equations (3.59)-(3.61) with the aid of equations (3.62) and (3.64) give the following equations in $(n+1)$ unknowns $\Phi_i(\eta_{ik},p)$ as

$$\frac{1}{n_1}\sum_{k=0}^{n_1}\zeta_k\left[\frac{1}{\eta_{1k}-\xi_{1j}} + R_{11}(\eta_{1k},\xi_{1j},p)\right]\Phi_1(\eta_{1k},p) + \frac{1}{n_2}\sum_{k=0}^{n_2}\zeta_k\left[\frac{1}{\eta_{2k}-z_{12}(\xi_{1j})} + \frac{1}{\eta_{2k}-g_{12}(\xi_{1j})} + R_{12}(\eta_{2k},\xi_{1j},p)\right]\Phi_2(\eta_{2k},p)$$

$$= \frac{T_{11}(\xi_{1j})}{\lambda_0 p}, \qquad j = 1, ..., n_1, \tag{3.65}$$

$$\frac{1}{n_1}\sum_{k=0}^{n_1}\zeta_k \left[\frac{1}{\eta_{1k} - z_{21}(\xi_{2j})} + R_{21}(\eta_{1k}, \xi_{2j}, p)\right] \Phi_1(\eta_{1k}, p)$$
$$+\frac{1}{n_2}\sum_{k=0}^{n_2}\zeta_k \left[\frac{1}{\eta_{2k} - \xi_{2j}} + \frac{1}{\eta_{2k} - g_{22}(\xi_{2j})} + R_{22}(\eta_{2k}, \xi_{2j}, p)\right] \Phi_2(\eta_{2k}, p)$$
$$= \frac{T_{12}(\xi_{2j})}{\lambda_0 p}, \qquad j = 1, ..., n_2, \tag{3.66}$$

$$\text{with} \qquad \sum_{k=0}^{n_i}\zeta_k \Phi_i(\eta_{ik}, p) = 0, \qquad i = 1, 2. \tag{3.67}$$

To get the numerical solution of the above system the Lobatto-Chebyshev collocation method and formulae in [44] are used to determine the crack tip DSIFs.

3.4 Driving force parameters

In the Laplace transformed domain, crack tip dynamic stress intensity factors (DSIFs) are defined as

$$K_{III}^{a*}(p) = \lim_{x \to a^+} \sqrt{2\pi(x-a)}\ \sigma_{yz}^{(2)*}(x, 0, p), \tag{3.68}$$

$$K_{III}^{b*}(p) = \lim_{x \to b^-} \sqrt{2\pi(b-x)}\ \sigma_{yz}^{(2)*}(x, 0, p), \tag{3.69}$$

$$K_{III}^{c*}(p) = \lim_{x \to c^+} \sqrt{2\pi(x-c)}\ \sigma_{yz}^{(2)*}(x, 0, p). \tag{3.70}$$

In terms of $\Phi_i(\eta_{ik}, p)$ $(k = 0, ..., n_i,\ i = 1, 2)$, the analytical expressions of crack tip DSIFs can be written as [66]

$$K_{III}^{a*}(p) = -\mu_2 \lambda_0 \sqrt{\pi a}\ \Phi_1(1, p), \tag{3.71}$$

$$K_{III}^{b*}(p) = \mu_2 \lambda_0 \sqrt{\pi(c-b)/2}\ \Phi_2(-1, p), \tag{3.72}$$

$$K_{III}^{c*}(p) = -\mu_2 \lambda_0 \sqrt{\pi(c-b)/2}\ \Phi_2(1, p). \tag{3.73}$$

To calculate numerical Laplace inversion of $K_{III}^{j*}(p)$ denoted by $K_{III}^{j}(t)$, $j = a, b, c$, the following series is used.

$$K_{III}^{j}(t) = \frac{1}{2}m_0^j(t) + \sum_{n=1}^{N_j} m_n^j(t), \qquad 0 \le t \le 2T^j, \tag{3.74}$$

$$\text{with} \quad m_n^j(t) = \frac{\exp(td^j)}{T^j}\,\Re\{\exp(in\pi t/T^j)K_{III}^{j*}(d^j + \frac{in\pi}{T^j})\},\ n = 0, 1, ...N_j,\ j = a, b, c, \tag{3.75}$$

where $i = \sqrt{-1}$, $p^j = d^j + in\pi/T^j$ and d^j is a real number greater than all the singularities of $\Re\{K_{III}^{j*}(p)\}$. The suitable choices of d^j, T^j, N_j can be found in [23]. The crack tip dynamic stress magnification factors (DSMFs) are determined by [79, 97]

$$M_{III}^{a}(t) = \frac{K_{III}^{a}(t)}{K_{0\,III}^{a}(t)}, \qquad M_{III}^{b}(t) = \frac{K_{III}^{b}(t)}{K_{0\,III}^{b}(t)}, \qquad M_{III}^{c}(t) = \frac{K_{III}^{c}(t)}{K_{0\,III}^{c}(t)}, \tag{3.76}$$

where $K_{0\,III}^{a}(t)$ is the dynamic stress intensity factor at $x = a$ due to the presence of central crack only, and $K_{0\,III}^{b}(t)$ and $K_{0\,III}^{c}(t)$ are the dynamic stress intensity factors at $x = b$ and $x = c$, respectively, due to the presence of outer cracks only.

3.5 Results and discussion

This section contains the study of the influences of the position of sudden impact loads, the thickness of the upper and lower strips, and crack axis positions on the interaction of three collinear Griffith cracks subject to anti-plane shear impact loading. Crack shielding and amplification phenomena are analyzed through the graphical presentations of DSMFs. The main interest of this study is the graphical presentations of the possibility of crack arrest during the interaction of collinear cracks in

different cases, as discussed. For numerical computation, $L = 20$ and $d = (c - b)/2$ are considered.

3.5.1 Impact of the position of impact load

In this section DSMFs, for impact load acting at the (a) upper material surface and (b) cracked surface, are calculated. It is assumed that the crack axis is in the middle of the FGM strip, i.e., $e = 0$ during numerical computation.

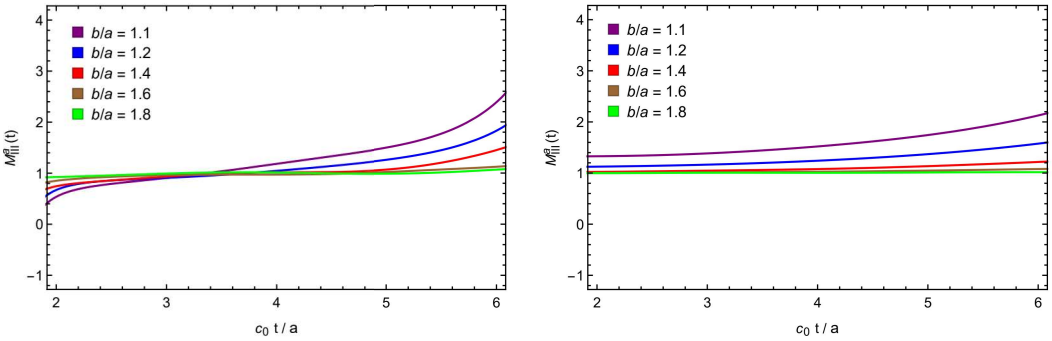

Figure 3.2: Variations in DSMF at the central crack tip a as a function of normalized time c_0t/a for distinct values of normalized outer crack tip b /a when sudden impact load is applied to the (a) upper material surface and (b) cracked surface.

For $h : h_0 : a = 1 : 1 : 0.5$, Figure 3.2 illustrates the transient response of DSMF M_a vs. normalized time c_0t/a for various values of dimensionless quantity b/a under the two mentioned loading positions. Keeping $a = 0.5, c = 1$ fixed and varying $b = 0.55, 0.6(0.1)0.9$, it is seen from the Figure 3.2b that in case of impact loads acting at the cracked surface when the outer crack approaches to central crack, DSMF at the crack tip $x = a$ increases with time. The amplification phenomenon ($M_a > 1$) is possible which are increased as the distance between the cracks decreases. Whereas for the case of impact loads acting at the upper material surface,

Figure 3.2a shows that as the length of the outer crack decreases M_a increases for $c_0t/a < 3$ and after that, it starts decreasing. In this case both shielding ($M_a < 1$) and amplification ($M_a > 1$) phenomena are observed. Due to shielding, there is a possibility of crack arrest.

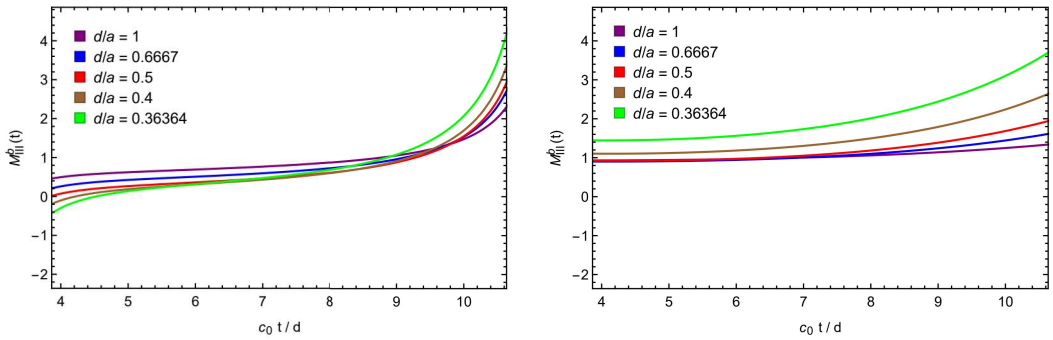

Figure 3.3: Variations in DSMF at the outer crack tip b as a function of normalized time c_0t/a for distinct values of normalized central crack tip $d\ /a$ when sudden impact load is applied to the (a) upper material surface and (b) cracked surface.

In Figures 3.3 and 3.4, the response curves of DSMFs M_b and M_c vs. normalized time c_0t/d with $h : h_0 : d = 1 : 1 : 0.2$ for various values of dimensionless quantity d/a under the two mentioned positions of impact loading are shown. Fixing $b = 0.6, c = 1$ and varying $a = 0.2(0.1)0.5, 0.55$, it is clear from the Figures 3.3b and 3.4b that in case of sudden impacts acting at the cracked surface as the length of central crack increases both M_b and M_c increase. In the case of applied load acts at the upper material surface, Figures 3.3a and 3.4a depict that as the length of the central crack increases, M_b and M_c decrease at first and after some time those are increased. Also Figures 3.3 and 3.4 show that under both loading conditions shielding ($M_b, M_c < 1$) as well as amplification ($M_b, M_c > 1$) both phenomena are possible and the effect of shielding changes to amplification with the increase in time.

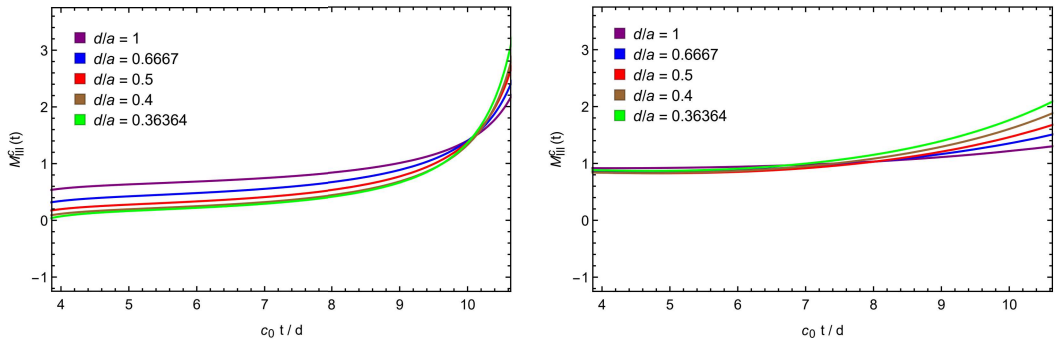

Figure 3.4: Variations in DSMF at the outer crack tip c as a function of normalized time c_0t/a for distinct values of normalized central crack tip $d\ /a$ when sudden impact load is applied to the (a) upper material surface and (b) cracked surface.

Therefore, the position of impact loading plays a significant role in affecting the interaction of collinear Griffith cracks. Also, the transient response of DSMFs obtained for impact load acting at the upper material surface shows interesting behavior due to its incremental and decremental nature.

3.5.2 Impact of thickness

The effect of the thickness of the three strips in the concerned mathematical model on the interaction of collinear cracks is discussed in this section. To investigate the thickness effect, three different cases are considered viz., $h_0 < h, h_0 = h$, and $h_0 > h$. DSMFs are calculated by fixing $e = 0$ and assuming that sudden impact load is applied at the upper material surface. For calculating M_a, $h : a = 1 : 0.5$ and for M_b and M_c, $h : d = 1 : 0.2$ are taken.

Figures (3.5a), (3.2a) and (3.5b) depict the response curves of M_a vs. normalized time c_0t/a for various values of dimensionless quantity b/a with $h_0 < h, h_0 = h$ and $h_0 > h$, respectively. Taking $a = 0.5, c = 1$ and varying $b = 0.55, 0.6(0.1)0.9$,

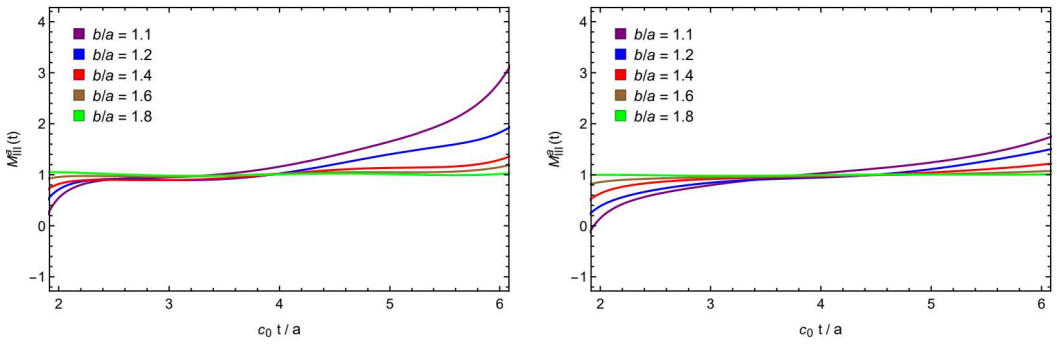

Figure 3.5: Plots showing DSMF at the central crack tip a as a function of normalized time c_0t/a for distinct values of normalized outer crack tip $b\ /a$ for normalized thickness (a) $h_0 : a = 0.5 : 0.5$ and (b) $h_0 : a = 2 : 0.5$.

it is seen from the figures that the behavior of M_a with normalized time is the same in all cases, i.e., as the length of outer crack increases M_a decreases and afterward the trend is increasing. For all three cases, both the shielding as well as amplification phenomena are observed during cracks' interaction. It is observed that $(M_a)_{h_0<h} > (M_a)_{h_0=h} > (M_a)_{h_0>h}$. It shows that even if the distance between the cracks is small, there is a possibility of a decrease in amplification with the increase in the thickness of the FGM strip, and as a result crack arrest may take place.

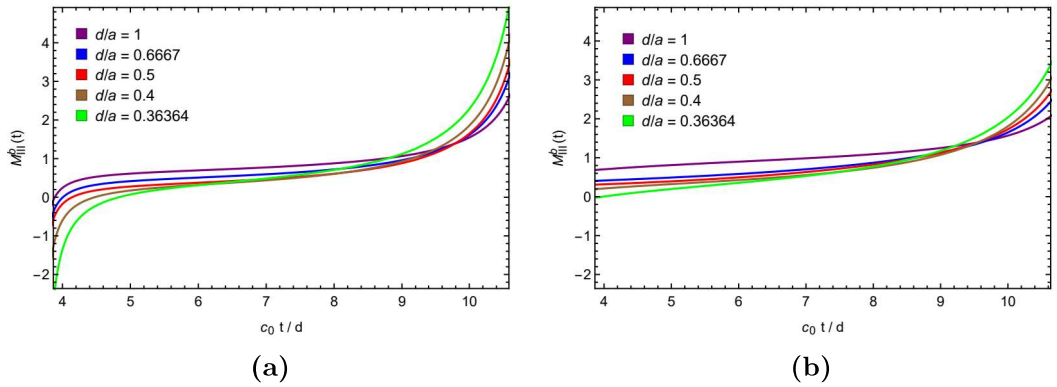

Figure 3.6: Plots showing DSMF at the outer crack tip b as a function of normalized time c_0t/a for distinct values of normalized central crack tip $d\ /a$ for normalized thickness (a) $h_0 : d = 0.5 : 0.2$ and (b) $h_0 : d = 2 : 0.2$.

For $h_0 < h, h_0 = h$ and $h_0 > h$, the response curves of M_b vs. normalized time c_0t/d for various values of dimensionless quantity b/a are shown in the Figures 3.6a, 3.3a and 3.6b respectively. Choosing $b = 0.6, c = 1$ and varying $a = 0.2(0.1)0.5, 0.55$, it is clear from the figures that in all three cases the behavior of response curves of M_b is similar to M_a i.e., as the length of the central crack increases M_b decreases and after some time it increases. In the case of M_b also there is a possibility of an increase in crack arrest as the thickness of the FGM strip and distance between cracks increases. It is clear from the Figures 3.7a, 3.4a and 3.7b that the behaviour of M_c is similar to M_b.

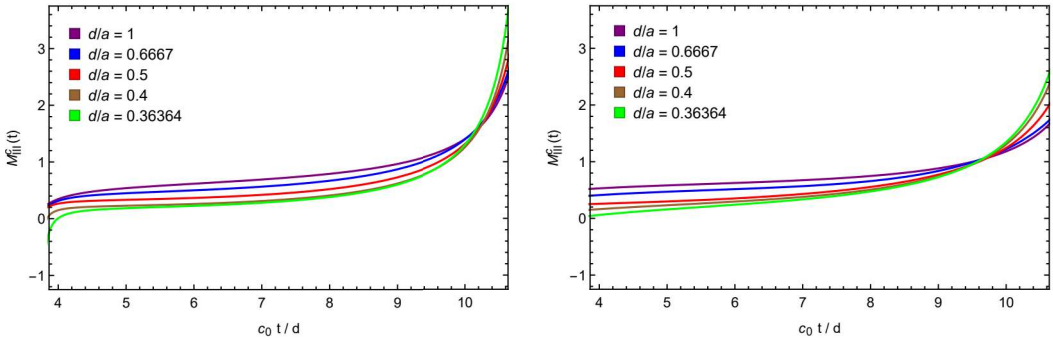

Figure 3.7: Plots showing DSMF at the outer crack tip c as a function of normalized time c_0t/a for distinct values of normalized central crack tip d/a for normalized thickness (a) $h_0 : d = 0.5 : 0.2$ and (b) $h_0 : d = 2 : 0.2$.

It can be concluded that the thicker the FGM strip, the stronger the possibility of crack arrest during the interaction of cracks. In other words, during cracks' interaction, the possibility of crack arrest is strong for thin outer strips.

3.5.3 Impact of the position of crack axis

To investigate the effect of crack axis position on the interaction of collinear cracks three different positions are considered, viz., $e = -h_0$, $e = 0$ and $e = h_0$ under the

condition that sudden impact load is applied at the upper material surface with $h : h_0 : a = 1 : 1 : 0.5$ for M_a and $h : h_0 : d = 1 : 1 : 0.2$ for M_b and M_c.

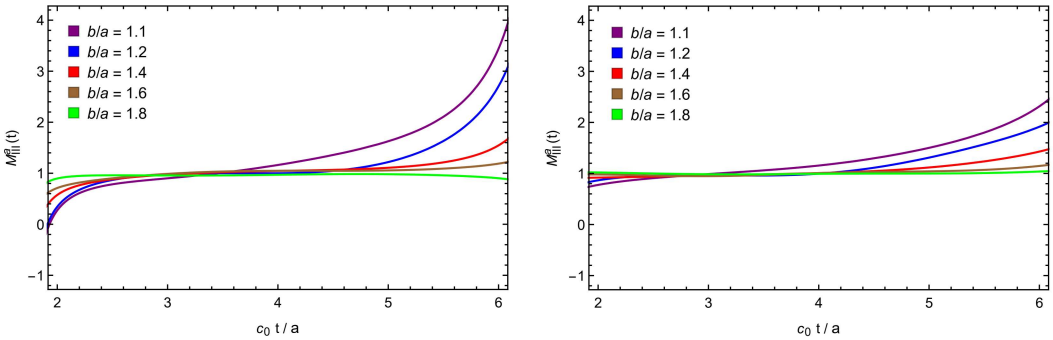

Figure 3.8: Influence of normalized time c_0t/a on DSMF at the central crack tip a for distinct values of normalized outer crack tip b /a when crack axis is located at the (a) lower interface $e = -h_0$ and (b) upper interface $e = h_0$.

For $a = 0.5, c = 1$ and $b = 0.55, 0.6(0.1)0.9$, it is observed from the Figures 3.8a, 3.2a and 3.8b that as the crack axis moves from the lower interface ($e = -h_0$) to the upper interface ($e = h_0$) along with decreasing length of outer crack, the effect of amplification decreases and possibility of crack arrest increases with normalized time c_0t/a.

Similarly, Figures 3.3a, 3.9, 3.4a and 3.10 illustrate that for $b = 0.6, c = 1$ and $a = 0.2(0.1)0.5, 0.55$, the nature of M_b and M_c is similar to M_a, i.e., with the increase in length of central crack and shifting of crack axis position from upper to lower interface, the possibility of crack arrest decreases with the normalized time c_0t/d.

Therefore it infers that the position of the crack axis affects the interaction of collinear cracks. During cracks' interaction, if the axis is closed to the upper interface, the possibility of crack arrest will be higher.

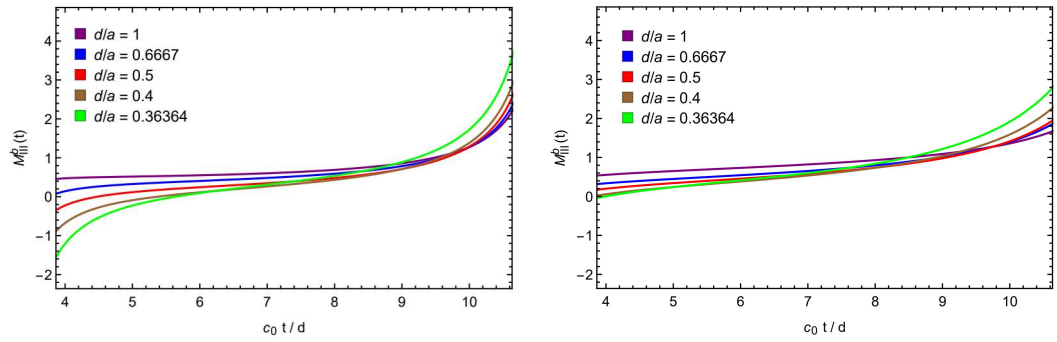

Figure 3.9: Influence of normalized time c_0t/a on DSMF at the outer crack tip b for distinct values of normalized central crack tip $d\ /a$ when crack axis is located at the (a) lower interface $e = -h_0$ and (b) upper interface $e = h_0$.

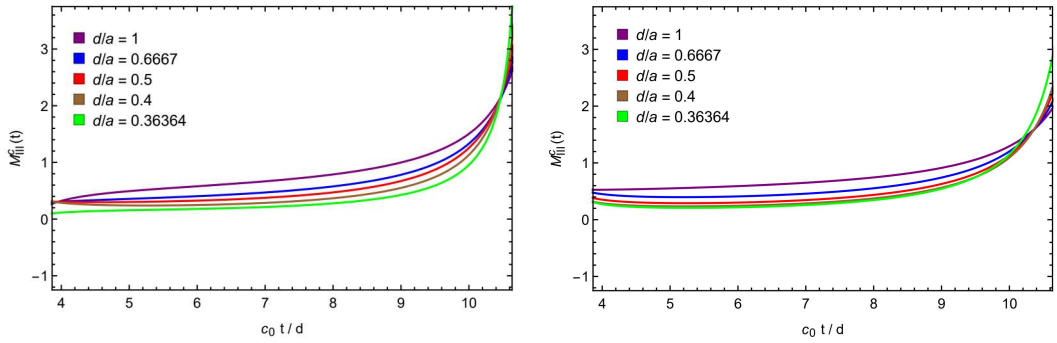

Figure 3.10: Influence of normalized time c_0t/a on DSMF at the outer crack tip c for distinct values of normalized central crack tip $d\ /a$ when crack axis is located at the (a) lower interface $e = -h_0$ and (b) upper interface $e = h_0$.

3.6 Concluding remarks

The goal of the current study is to develop the understanding of the possibility of crack arrest caused by the interaction of a central Griffith crack and two symmetrically positioned collinear Griffith cracks those are situated in a FGM strip. The FGM strip is joined between two different elastic strips. The study has succeeded in achieving the following objectives:

1. At the tips of the collinear cracks, the expressions of DSIFs and DSMFs are obtained. The expressions of DSMFs have been used to determine the occurrences of shielding (DSMFs < 1) and amplification (DSMFs > 1) phenomena.

2. When the thickness of each strip is identical and the crack's axis is in the middle of the FGM strip, the graphical displays of DSMFs vs. normalized time for two distinct positions of impact loading are shown. If a sudden impact load is applied to the upper material surface, the interaction effect has both amplification and shielding phenomena, whereas only the amplification effect is shown to occur when the impact load is applied to the cracked surface. Consequently, the impact loading position has a major impact on the interaction of collinear cracks.

3. When the crack's axis is in the middle of the FGM strip and an impact load is being applied to the upper surface of the material, the pictorial presentations of DSMFs vs. normalized time are shown for varying thicknesses of the FGM strip. Again if the outer cracks present in a thick FGM strip, there is a possibility of the crack arrest.

4. The likelihood of crack arrest is higher when the upper and lower elastic strips are thinner.

5. When the thickness of each strip is the same and the crack's axis is in the middle of the FGM strip, the graphical presentations of DSMFs vs. normalized time are presented for various positions of the crack's axis. The possibility of crack arrest increases as the crack axis moves from the lower to the upper interface.

****